

THE ULTRALUMINOUS X-RAY SOURCE NGC 1313 X-2 (MS 0317.7-6647) AND ITS ENVIRONMENT

LUCA ZAMPIERI, PAOLA MUCCIARELLI¹, RENATO FALOMO

INAF-Osservatorio Astronomico di Padova, Vicolo dell’Osservatorio 5, I-35122 Padova, Italy

PHILIP KAARET

Harvard-Smithsonian Center for Astrophysics, 60 Garden Street, Cambridge, MA 02138

ROSANNE DI STEFANO

Harvard-Smithsonian Center for Astrophysics, 60 Garden Street, Cambridge, MA 02138

Department of Physics and Astronomy, Tufts University, Robinson Hall, Medford, MA 02155

ROBERTO TUROLLA

Dipartimento di Fisica, Università di Padova, Via Marzolo 8, I-35131 Padova, Italy

MATTEO CHIEREGATO, ALDO TREVES

Dipartimento di Scienze, Università dell’Insubria, Via Valleggio 11, I-22100 Como, Italy

Draft version October 26, 2018

ABSTRACT

We present new optical and *Chandra* observations of the field containing the ultraluminous X-ray source NGC 1313 X-2. On an ESO 3.6 m image, the *Chandra* error box embraces a $R = 21.6$ point-like object and excludes a previously proposed optical counterpart. The resulting X-ray/optical flux ratio of NGC 1313 X-2 is ~ 500 . The value of f_X/f_{opt} , the X-ray variability history and the spectral distribution derived from a re-analysis of the *ROSAT*, *ASCA* and *XMM* data indicate a luminous X-ray binary in NGC 1313 as a likely explanation for NGC 1313 X-2. If the X-ray soft component observed in the *XMM* EPIC spectrum originates from an accretion disk, the inferred mass of the compact remnant is $\approx 100 M_\odot$, making it an intermediate mass black hole. The derived optical luminosity ($L \approx 10^5 L_\odot$) is consistent with that of a $\approx 15 - 20 M_\odot$ companion. The properties of the environment of NGC 1313 X-2 are briefly discussed.

Subject headings: galaxies: individual (NGC 1313) — stars: individual (NGC1313 X-2/MS 0317.7-6647) — X-rays: binaries — X-rays: galaxies

1. INTRODUCTION

First revealed by the *Einstein* Observatory (see e.g. Fabbiano 1989), point-like, off-nuclear X-ray sources with luminosities significantly exceeding the Eddington limit for one solar mass are being progressively discovered in the field of many nearby galaxies. To date, hundreds of such sources have been found in dozens of galaxies, both ellipticals and spirals (e.g. Colbert & Ptak 2002). These powerful objects, commonly referred to as ultraluminous X-ray sources (ULXs), do not appear to have an obvious Galactic counterpart. Despite some of them have been identified with supernovae or background active galactic nuclei, the nature of most of these sources remains unclear. X-ray spectra have been obtained with the *Einstein*, *ROSAT*, *ASCA* and recently *XMM-Newton* and *Chandra* satellites. Although the statistics is rather poor, in many cases fitting with simple models indicates that the spectral properties are consistent with those of Galactic black hole binaries (e.g. Foschini et al. 2002a). About half of them show some degree of variability in the X-ray flux. Among the various possibilities, the most favored explanation is that ULXs are powered by accretion and that they are somewhat special X-ray binaries, either containing an intermediate mass black hole (BH) with $M_{BH} \gtrsim 100 M_\odot$ (e.g. Colbert & Mushotzky 1999; Kaaret et al. 2001) or

having beamed emission toward us (e.g. King et al. 2001; Kaaret et al. 2003). For a recent review on the properties of ULXs we refer to Fabbiano & White (2003).

Optical observations are of fundamental importance to better assess the nature of these sources but they are still rather scarce (see e.g. Cagnoni et al. 2003; Foschini et al. 2002b). Some ULXs have optical counterparts in the Digitized Sky Survey or Hubble Space Telescope images (e.g. NGC 5204 X-1; Roberts et al. 2001; Goad et al. 2002) and some appear to be embedded in emission nebulae a few hundred parsecs in diameter (Pakull & Mirioni 2002).

NGC 1313 X-2 was one of the first sources of this type to be found. It was serendipitously discovered in an *Einstein* IPC pointing toward the nearby SBc galaxy NGC 1313 (Fabbiano & Trinchieri 1987). Originally included in the *Einstein* Extended Medium Sensitivity Survey as MS 0317.7-6647, it is located $\sim 6'$ south of the nucleus of NGC 1313. Stocke et al. (1995) investigated the nature of MS 0317.7-6647 on the basis of X-ray, optical and radio observations. They identified a possible optical counterpart and concluded that the source could be either a Galactic isolated neutron star or a binary containing a massive BH in NGC 1313. Spectral fits to *ROSAT* PSPC data (Stocke et al. 1995; Colbert et al. 1995; Miller et al. 1998) yielded results consistent with many single compo-

¹ Also at SISSA, Via Beirut 2-4, I-34014 Trieste, Italy

ment models. *ASCA* observations (Petre et al. 1994; Makishima et al. 2000) are described successfully by a multi-color disk blackbody (MCD) model, representing thermal emission from a standard accretion disk around a BH. A very recent analysis of a *XMM* EPIC-MOS observation of NGC 1313 (Miller et al. 2003) indicates that two spectral components, soft and hard, are required to fit the spectrum of NGC 1313 X-2 and the normalization of the soft component yields a conspicuous mass of the black hole $M_{BH} \gtrsim 830M_{\odot}$.

We present new optical² and *Chandra* observations of NGC 1313 X-2, with the aim to shed further light on its enigmatic nature. In § 2 we present *Chandra* data and re-analyze all the available X-ray observations of NGC 1313 X-2. In § 3 optical observations of the field of this ULX are reported. Finally, the implications of our results on the nature of NGC 1313 X-2 are discussed in § 4.

2. X-RAY DATA

NGC 1313 X-2 was first observed by *Einstein* with the IPC instrument in 1980. It was then pointed several times by *ROSAT* (PSPC and HRI) between 1991 and 1998 (Stocke et al. 1995; Colbert et al. 1995; Miller et al. 1998; Schlegel et al. 2000), by *ASCA* (SIS and GIS) in 1993 and 1995 (Petre et al. 1994; Makishima et al. 2000) and by *XMM* (EPIC) in 2000 (Miller et al. 2003). Most recent data are from a 2002 *Chandra* (ACIS-S) pointing, reported here for the first time. The *Chandra* observation began on 13 Oct 2002 and had a duration of 19.9 ks. The primary goal of the observation was to study sources near the center of the galaxy, but the aim-point was adjusted to also place NGC 1313 X-1, NGC 1313 X-2, and SN 1978K on the S3 chip of the ACIS-S. In addition, we present here a complete analysis of the *XMM* observation, including the EPIC-PN data, which were not considered by Miller et al. (2003).

2.1. X-ray astrometry

An accurate determination of the X-ray position of NGC 1313 X-2 can be obtained from the 2002 *Chandra* pointing, using the *Chandra* aspect solution. Chandra data were extracted from the S3 chip on the ACIS-S and subjected to standard processing and event screening. No strong background flares were found, so the entire observation was used. Because the source is 5' off axis, the point spread function was fitted with an ellipsoidal Gaussian (1.9" and 1.1" along the two axes, rms values). Also, the pixel with the highest number of counts is offset by 0.8" from the center of the fitted ellipse. Taking these uncertainties into account, we conservatively estimate a positional error of 0.7" (1- σ). The final *Chandra* position is: $\alpha = 03h 18m 22.27s \pm 0.12s$, $\delta = -66^{\circ} 36' 03.8'' \pm 0.7''$.

In order to check the accuracy of the *Chandra* aspect solution, we exploited the presence in the field of view of a quite peculiar supernova, SN 1978K, that shows powerful radio and X-ray emission. The *Chandra* position of SN 1978K is $\alpha = 03h 17m 38.69s$, $\delta = -66^{\circ} 33' 03.6''$ (J2000), within 0.46" from the accurate (0.1") radio position of Ryder et al. (1993). This is consistent with the expected *Chandra* aspect accuracy.

The position of NGC 1313 X-2 was previously determined from the *ROSAT* HRI (Stocke et al. 1995; Schlegel et al. 2000) and *XMM* EPIC-MOS (Miller et al. 2003) images. Typical 1- σ error boxes are $\sim 3''$ for *ROSAT* HRI and $\sim 2''$ for *XMM* EPIC-MOS. The *ROSAT* and *XMM* positions and corresponding error boxes are summarized in Table 1.

2.2. X-ray spectrum and lightcurve

We analyzed the *XMM* EPIC data from both the MOS and PN cameras (operated with the medium filter). The EPIC-PN spectrum is reported here for the first time and was extracted directly from the observation data file because the automatic pipe-line processing failed to produce a standard event list for the EPIC-PN camera. Both reduction procedures (`epchain` and `epproc`) were used to extract the data obtaining similar results (differing typically by a few percents). Data screening, region selection and event extraction were performed using standard software (XMMSELECT v 2.43.2). An analysis of the MOS and PN light curves shows that solar flares are present in both datasets. They were filtered out using the standard criterion (total off-source count rate above 10 keV < 5 counts s $^{-1}$ for MOS and < 15 counts s $^{-1}$ for PN). We extracted the source counts from a circle of 40" and 30" for the MOS and PN cameras, respectively. The proximity of the source to one of the CCD edges in the EPIC-MOS data requires some care. We eliminated the area of a box aligned and superimposed to the CCD boundary to avoid contamination from bad pixels close to the source. The background was selected from a circle of 60" in a nearby source-free region of the same CCD. Ancillary and response files were produced using the appropriate XMMSELECT tasks. Data were grouped to require at least 20 counts per bin for the MOS data and 40 counts per bin for the PN data, and were then analyzed and compared with different models using XSPEC (v 11.2.0). To minimize the effects of possible relative calibration uncertainties, the fit of the MOS1, MOS2 and PN spectra were performed with an overall normalization constant (those of the two MOS cameras differ by $\sim 10\%$, while that of the PN instrument is larger by $\sim 25\%$). The count rates are 0.08 counts s $^{-1}$ for the MOS cameras and 0.25 counts s $^{-1}$ for the PN.

In order to reconstruct the X-ray variability history of NGC 1313 X-2, we have carefully re-analyzed also the *ROSAT* and *ASCA* observations. Extraction regions for the *ASCA* SIS data were chosen with care to avoid contamination from the CCD edges and SN 1978K. Spectra were grouped to require at least 15 counts per bin for the *ROSAT* data and 20 counts per bin for the *ASCA* data.

The results of the spectral analysis are listed in Table 2. The statistics of the *XMM* EPIC spectrum is significantly improved including the EPIC-PN data (the PN camera has almost twice more counts than each single MOS instrument). An absorbed power-law does not provide a satisfactory fit of the joint MOS1, MOS2 and PN spectra ($\chi^2_{red} = 1.2$ for 249 d.o.f.). Two components models provide a significant improvement over single component ones. The best fit is obtained with an absorbed soft, thermal component plus a power-law. Adding a MCD model to the power-law results in an improvement of the fit which is

² Based on observations collected at the European Southern Observatory, Chile, Program number 68.B-0083(A).

significant at the $\sim 4.5/5$ (epchain/epproc) σ level. Figure 2 shows the results for a MCD+power-law fit. The resulting best fitting parameters are $kT = 200^{+50}_{-40}$ eV, $\Gamma = 2.23^{+0.15}_{-0.09}$ and $N_H = 3.13^{+0.92}_{-0.37} \times 10^{21}$ cm $^{-2}$ for the inner disk temperature, photon index and column density, respectively (see Table 2). There are residuals in the fit (mainly in the EPIC-PN spectrum) that suggest the possible presence of emission lines. We emphasize that the EPIC-PN data provide marginal evidence for the presence of a soft component even at low metallicities. Reducing the abundances of the absorbing gas at 0.5 solar, a simple power-law fit of the EPIC-PN data has $\chi^2_{red} = 1.24$ (89 d.o.f.), while a MCD+power-law fit gives $\chi^2_{red} = 1.15$ (87 d.o.f.). Finally, it is worth noting that the value of kT is $\sim 25\%$ larger (although consistent within 1- σ) than that derived by Miller et al. (2003).

In Figure 1 we report the X-ray flux derived from all the available observations of NGC1313 X-2. The fluxes were consistently derived from the best fit parameters of the X-ray spectral analysis reported in Table 2. An approximate estimate of the errors, based on counting statistics, is 5-10%. The *Chandra* point is not included in Figure 1 because of pile-up problems. The unabsorbed 0.2–10 keV flux from both the *XMM* EPIC-MOS and PN instruments agree within $\sim 20\%$ and give an average value of 2.4×10^{-12} erg cm $^{-2}$ s $^{-1}$. This value is lower by a factor ~ 2 than that estimated by Miller et al. (2003). Variability of up to a factor 2 on a timescale of months is clearly present and it is reminiscent of the behavior observed in Galactic X-ray binaries. If uncertainties in the best-fitting spectral parameters are taken into account, the amplitude of variability is reduced but not eliminated. This suggests that a compact object is present in NGC 1313 X-2. If the emission is isotropic and the distance is that of the host galaxy ($\simeq 3.7$ Mpc; Tully 1988), the X-ray luminosity in the 0.2–10 keV range is $L_X \simeq (3 - 6 \pm 0.5) \times 10^{39}$ erg s $^{-1}$. If at maximum the source radiates at the Eddington limit L_{Edd} , the BH mass is $\sim 50 M_\odot$. Sub-Eddington accretion would imply an even larger mass.

Interestingly, comparing data from the first and second epoch *ASCA* observations, the X-ray flux of NGC 1313 X-2 appears to increase with increasing spectral hardness (see Table 2). This behavior is similar to that observed in the ULXs of the Antennae galaxy (Fabbiano et al. 2003) and is opposite to what is usually seen in Galactic BH X-ray binaries (e.g. Cyg X-1).

3. OPTICAL OBSERVATIONS

Optical images of the field of NGC 1313 X-2 in the *R*-band (Bessel filter) were taken on 16 January 2002 with the 3.6 m telescope of the European Southern Observatory (ESO) at La Silla (Chile). We used EFOSC2 with a Loral/Lesser CCD of 2048×2048 pixels yielding a field of view of $\sim 5' \times 5'$ at a resolution of 0.314''/pixel (re-binned by a factor 2). The night was clear with a seeing of about 1''. Four images were obtained for a total exposure time of 1320 s. Standard reduction of the data (including bias subtraction and flat-field correction) was performed within the IRAF (v 2.12) environment.

A spectrum of one of the field objects (object A; see below) was secured on the same night. We performed low-resolution (13.4 Å, grism#4) spectroscopy for a total expo-

sure time of 1200 s. After applying standard corrections and sky subtraction, cosmic rays were removed and the spectrum was corrected for atmospheric extinction. At the time of the optical observations object A had already been imaged at the 1.1 m Las Campanas telescope by Stocke et al. (1995) and was considered a possible counterpart of NGC 1313 X-2. Although the new accurate *Chandra* position rules out an association with this object (see below), the spectrum can be used to gain insight on the properties of a surrounding nebula, possibly associated with the X-ray source (see e.g. Pakull & Mirioni 2002).

3.1. Astrometry and photometry of field objects

Our four ESO images were astrometrically calibrated using an IRAF task (PLTSOL) and performing a polynomial interpolation starting from the positions of GSC2 ESO field stars. The internal accuracy of this procedure was estimated comparing the actual positions of a number of GSC2 stars not used for astrometric calibration with the positions contained in the catalog. The accuracy is 0.3'' (1- σ). The four calibrated images were then summed together and the resulting image is shown in Figure 3.

In order to check for the relative systematics between the optical and X-ray astrometric calibrations, we used again the position of SN 1978K. This supernova is inside the *Chandra* field of view but outside our optical image. Thus, we analyzed also an archival image of SN 1978K (from the Padova-Asiago Supernova Archive) taken on 13 September 1999 with the same telescope and a similar instrumental set-up (ESO 3.6m+EFOSC/2.9+R#642, exposure time 180 s). After calibrating the archival image, the position of SN 1978K is $\alpha = 03h 17m 38.605s$, $\delta = -66^\circ 33' 03.13''$ (J2000). This is within 0.28'' from the radio position of Ryder et al. (1993), improving significantly upon the previous optical position by the same authors. The difference between the centroids of the optical and *Chandra* positions of SN 1978K is 0.69'' ($\alpha_{opt} - \alpha_X = -0.085s$, $\delta_{opt} - \delta_X = -0.47''$). Although this difference is small and comparable with the statistical errors, we decided to apply this correction to the *Chandra* position of NGC 1313 X-2 to eliminate any systematic error between the optical and X-ray astrometric calibrations. The resulting *Chandra* position of NGC 1313 X-2 is reported in Table 1.

The photometry of the objects in our optical image was performed calibrating the frame with the *R*-band magnitudes of 23 stars from the SuperCosmos Sky Survey (Hambly, Irwin & MacGillivray 2001) homogeneously distributed over the field of view. The internal accuracy of this calibration is 0.2 mag. Aperture (5'' radius) magnitudes are reported in Table 1.

3.2. Spectroscopy of the emission nebula

The two-dimensional spectrum of the field around object A (Figure 4) shows clear emission lines extending for tens of arcsecs from east to west, confirming the existence of an extended (~ 400 pc) optical emission nebula that was first found in deep H α images by Pakull & Mirioni (2002). A one-dimensional spectrum of the field was extracted over an aperture of 0.9'' (3 pixels) from two regions east-ward and west-ward of the position of object A and adjacent to it (Figure 5). Wavelength and relative flux calibration were applied to the data. The one-dimensional

spectrum shows strong emission lines of H_α , H_β , [SII] $\lambda\lambda$ 6717–6731 Å, [OI] λ 6300 Å and [OIII] $\lambda\lambda$ 4959–5007 Å. The shift of the centroid of the lines (~ 10 Å) is consistent with the recession velocity of the galaxy and indicates that the emission nebula is located in NGC 1313.

It is worth emphasizing the abrupt change in the absolute and relative intensity of the emission lines from east to west, indicating variations in the physical conditions and/or geometry of the emission nebula. In particular, strong emission from [OIII] is present on the east side but almost absent on the west side, while emission from H_α , [SII], [OI] and other elements is present on the west side but weaker or absent on the east side. A careful inspection of the line intensity profiles (in particular those of H_α and [SII]) reveals a fairly symmetric, broadly peaked profile, centered at $\sim 2''$ west of the position of object A, and a weaker, roughly constant intensity component extending in the east direction.

4. DISCUSSION

Our *Chandra* position of NGC 1313 X-2 (Table 1) is shown in Figure 3, together with the *ROSAT* HRI (Schlegel et al. 2000) and *XMM* EPIC-MOS (Miller et al. 2003) error boxes, overlaid on our ESO image. All measurements are consistent within $1-\sigma$. The distance of the centroids of objects A, B and D with respect to the *Chandra* position is $3.6''$, $4.1''$ and $7.3''$, respectively. Even taking into account the statistical error on the optical positions ($0.3''$), these three objects can be ruled out at a significance level of at least $3-\sigma$. On the other hand, object C is inside the *Chandra* error box and its position coincides within $1-\sigma$ with that of NGC 1313 X-2, making it a likely counterpart.

From the maximum absorbed X-ray flux of NGC 1313 X-2 ($f_X \sim 2 \times 10^{-12}$ erg cm $^{-2}$ s $^{-1}$) and optical magnitude of object C ($R = 21.6$), we estimate $f_X/f_{opt} \sim 500$. This value is very high, in agreement with the suggestion by Cagnoni et al. (2002) that ULXs can be selected on the basis of their large f_X/f_{opt} . Only Isolated Neutron Stars (INSs), heavily obscured AGNs and luminous X-ray binaries can reach such large values of the X-ray/optical flux ratio. INSs are extreme in this respect, with $B \approx 25$ optical counterparts and typical X-ray-to-optical flux ratios $\gtrsim 10^5$ (see e.g. Kaplan, Kulkarni & van Kerkwijk 2003). The presence of the relatively bright ($R \sim 21.6$) object C in the *Chandra* error box makes this possibility unlikely. Furthermore, known INSs exhibit different spectral properties with no significant variability. On the other hand, a heavily obscured AGN is expected to have a rather hard X-ray spectrum and to emit significantly in the near-infrared (see e.g. Brusa et al. 2002). Given the X-ray luminosity of NGC 1313 X-2, an infrared magnitude $K \approx 12$ is expected were it an obscured AGN. The lack of any IR counterpart on a K image of the 2MASS All Sky Image Service down to a limiting magnitude $K \simeq 14$ ($10-\sigma$) and the softer X-ray spectrum of NGC 1313 X-2 make this possibility unlikely, although a low resolution optical spectrum of object C is definitely required to settle this issue. Our accurate *Chandra* position and optical identification favor a very luminous X-ray binary in NGC 1313 as the likely explanation for NGC 1313 X-2. As a reference, the X-ray/optical flux ratio of persistent BH binaries at maximum is $\gtrsim 10 - 100$,

while that of soft X-ray transients in outburst can reach 2000 (Masetti 1997). This is in line with the alleged binary nature of ULXs and is consistent with the observed properties of this source, such as the X-ray variability and the observed X-ray spectrum, including the presence of a soft component probably produced by an accretion disk.

If indeed NGC 1313 X-2 is a black hole binary, the X-ray spectral parameters, in particular the temperature of the MCD fit (hereafter referred to as T_{MCD}), can be used to estimate the BH mass. This is similar to what done by Miller et al. (2003) using the normalization of the MCD fit and, as discussed below, we reach similar conclusions. The effective temperature of a standard accretion disk depends on radius as $T^4 = (3GM_B \dot{M}/8\pi\sigma r_{in}^3)(r_{in}/r)^{3/4}[1 - (r_{in}/r)^{1/2}]$, where \dot{M} is the accretion rate and r_{in} is the innermost disk radius (e.g. Frank, King & Raine 1980). Assuming that T_{MCD} represents an estimate of the maximum disk temperature, it is $(3GM_B \dot{M}/8\pi\sigma r_{in}^3)^{1/4} = \alpha T_{MCD}$, with $\alpha \simeq 2$. Neglecting relativistic corrections and assuming that the disk terminates at the innermost stable circular orbit of a Schwarzschild BH, it is: $M_B/M_\odot = (\dot{M}c^2/L_{Edd})f^4(\alpha T_{MCD}/1.5 \times 10^7 \text{ K})^{-4}$, where f is a color correction factor ($f \sim 1.6 - 1.7$, Shimura & Takahara 1995; Zampieri, Turolla & Szuszkiewicz 2001). Given the strong dependence of M_B on temperature, any uncertainty in the accretion physics and radiative transfer may induce significant errors in the resulting value of M_B . So, the inferred spectroscopic measurement of the BH mass should be taken simply as an approximate estimate. The low inner disk temperature obtained from the two-components fit to the *XMM* EPIC spectrum ($kT \sim 200$ eV) implies $M_B \approx 90f^4 M_\odot$ ($\alpha \simeq 2$) for Eddington limited accretion, somewhat larger than that derived from the flux. This result removes the need for a rapidly spinning BH (invoked by Makishima et al. 2000 from an analysis of the *ASCA* data) and agrees with the conclusion of Miller et al. (2003) that NGC 1313 X-2 contains an intermediate mass BH. The large inferred BH mass does not require beamed emission. Then, the estimated accretion rate (assuming 10% efficiency) is $\dot{M} \sim 10^{-7} M_\odot \text{ yr}^{-1}$, forcing the mass reservoir to be a companion star.

From the apparent magnitude ($R = 21.6$) and absorption ($A_R \simeq 1.7$, computed from the X-ray best fitting column density $N_H \sim 3 \times 10^{21}$ cm $^{-2}$; Bohlin et al. 1978) of object C, we estimate an absolute magnitude $M_R \simeq -7.9$ and a luminosity in the range $\sim 7 \times 10^4 - 10^6 L_\odot$, depending on the adopted bolometric correction. If this originates from the companion star, the inferred luminosity is consistent with a $\approx 20M_\odot$ main sequence star or a $\sim 15 - 20M_\odot$ evolved OB supergiant (e.g. Bowers & Deeming 1984), making NGC 1313 X-2 a high-mass X-ray binary. In luminous Galactic X-ray binaries, the reprocessed optical emission from the disk may be significant. Assuming that 20–30% of the X-ray flux produced in the innermost part of the accretion disk intercepts the outer regions, for realistic values of the albedo ($\gtrsim 0.9$; e.g. de Jong, van Paradijs & Augusteijn 1996) few percents of the X-ray luminosity ($\approx 10^{38}$ erg s $^{-1}$) can be absorbed and re-emitted in the optical band. Characteristic emission lines of X-ray-ionized H, He or N, typically seen in luminous Galactic X-ray binaries should then be detectable in the optical spectrum. Also X-ray heating of the companion star itself may con-

tribute to the optical emission. If the optical luminosity comes in part from X-ray re-irradiation, the mass of the companion would be lower. Taking $M_2 \sim 20M_\odot$ as an upper limit for the mass of the companion, the mass ratio of the binary is $q = M_2/M_{BH} \lesssim 0.4f^{-4} \ll 1$. Writing the binary separation as $a = 2.16R_2[q/(1+q)]^{-1/3}$ (Paczynski 1971), the orbital period of the system is $P \gtrsim 0.15(R_2/100R_\odot)^{3/2}f^2(M_{BH}/50M_\odot)^{-1/2}$ yr. According to King et al. (2001), the system should not be a persistent X-ray source.

Although difficult to reconcile with the properties of the environment surrounding NGC 1313 X-2 (see below), we can not rule out also that the optical emission detected in the *Chandra* error box originates from a stellar cluster (see e.g. the case of a ULX in NGC 4565; Wu et al. 2002), in which case NGC 1313 X-2 may be a low-mass X-ray binary in the cluster.

The mass accretion rate required to produce the observed luminosity may in principle be provided by Roche-lobe overflow from an evolved companion or by a wind from a supergiant. In the first case, evolutionary swelling of the companion keeps pace with the increase in Roche lobe size and the system remains self-sustained: accretion is likely to proceed through a disk. In the second case, assuming 10% accretion efficiency and that the BH can capture $\sim 1\%$ of the mass outflow, the wind must be very powerful ($\dot{M} \sim 10^{-5}M_\odot\text{ yr}^{-1}$). A lower efficiency would require too high a gas supply, so a disk is needed even in a wind-fed system. In this case, however, the disk is probably much smaller than in a Roche-lobe overflow system and the optical emission dominated by the supergiant. On the other hand, in a Roche-lobe overflow system, an extended, possibly re-irradiated accretion disk should contribute heavily in the UV and *B* bands, producing strong emission lines. Thus, the two modes of mass supply are likely to be distinguishable by optical spectroscopy.

We now turn to discuss how our optical observations can be used to constrain the environment of NGC 1313 X-2. Figures 4 and 5 reveal that NGC 1313 X-2 is likely to be associated with an optical emission nebula, recognizable also in a H_α image taken by Pakull & Mirioni (2002). From the velocity (80 km s^{-1}) and flux of H_β , they derive an impressive mechanical energy of $3 - 10 \times 10^{52}\text{ erg}$ for the expanding ionized gas, and suggest that the nebula is inflated by a relativistic jet from NGC 1313 X-2. Our measured ratio of $[\text{SII}]/H_\alpha$ (~ 0.5) is consistent with that expected from a shock-ionized supernova remnant, a stellar wind-shocked nebula or diffuse ionized gas (Matonick & Fesen 1997). However, the inferred diameter and energy of the nebula are too large to be consistent with a single supernova event, unless it was produced by a hypernova similar to SN 1998bw (see e.g. Iwamoto et al. 1998). In fact, it could be the result of several explosion events (multiple supernova remnant) or be originated by the intense wind of hot stars, possibly the parent stellar association of NGC 1313 X-2. As discussed in the previous section, the nebula appears to have some internal structure: a comparatively brighter, fairly symmetric component west of the position of NGC 1313 X-2 and a weaker, slightly elongated one extending in the east direction. The brighter part of the nebula has $[\text{SII}]/H_\alpha = 0.58$, the weaker one has $[\text{SII}]/H_\alpha = 0.44$ and intense $[\text{OIII}]$ emission. Different possibilities may ex-

plain the irregular appearance of the nebula. As suggested by Pakull & Mirioni (2002), the varying line intensity may be caused by reprocessed emission from the X-ray ionized interstellar medium where the physical conditions (in particular the density) vary on a scale ~ 100 pc. However, the nebular emission may also arise from two physically distinct components: a wind-shocked nebula produced by a possible parent stellar association of NGC 1313 X-2 and a multiple supernova remnant. This hypothesis seems to be confirmed also by the marginal detection of (possibly extended) UV emission in an image of the *XMM* Optical Monitor (see Figure 6), in coincidence with the brighter component. Clearly, the weaker component may still be a jet-inflated nebula, as suggested by Pakull & Mirioni (2002). Finally, we note that, although NGC 1313 X-2 is somewhat hotter and much more luminous, the $[\text{OIII}]$ signature in the eastern portion of the nebula is reminiscent of predictions for the radiation-limited nebulae around supersoft sources (Di Stefano, Paerels & Rappaport 1995; Chiang & Rappaport 1996).

It is interesting to note that object A, the possible association of which with NGC 1313 X-2 was discussed by Stocke et al. (1995), lies very close both to the *Chandra* error box and the point where the intensity of the nebular emission lines suddenly changes. The continuum spectrum of this object, obtained after subtracting off the emission line spectrum of the nebula in the adjacent regions, was compared to template stellar spectra (Pickles 1998) and turns out to be in fair quantitative agreement with that of a G-M supergiant, but not with that of late-type dwarfs. This result is independent of reddening. The absolute magnitude of object A is $M_R \simeq -9.7$, and the luminosity $L \sim 5 \times 10^5L_\odot$ (assuming a bolometric correction appropriate for a K star). Object A may be a very massive ($\sim 30M_\odot$) G-M supergiant of radius $\sim 1000R_\odot$ or a cluster in NGC 1313. The first interpretation would support the conclusion that the region in which NGC 1313 X-2 is located is an active star forming region, in which the initial mass function is top-heavy. On the other hand, the second possibility appears more likely because $\sim 30M_\odot$ massive stars are extremely rare. However, the red color would indicate a rather evolved cluster that would be projected by chance on the active star forming environment in which NGC 1313 X-2 appears to be embedded.

A crucial question is how a binary system containing an intermediate mass BH may have formed (see e.g. van der Marel 2003). The BH progenitor must have been rather massive. This is consistent with the fact that NGC 1313 is likely to have lower than solar metallicity ($Z \sim 0.5$; Zaritsky, Kennicutt & Huchra 1994) and hence mass loss was less intense. Such a massive BH may have formed through direct collapse without producing a supernova. In this way, if the system was born as a binary, it may have survived after the collapse of the primary. Although less likely, it is also possible that the companion might have been captured from a nearby stellar association. In this case, it is not possible to exclude that the BH may have formed from an early episode of star formation (population III).

It is worth noting that, although the large BH mass does not require that the emission is beamed, we cannot rule out that a moderate jet activity, producing radio emission

(and possibly inflating the emission nebula), is present in NGC 1313 X-2 (see e.g. the case of an ULX in NGC 5408; Kaaret et al. 2003). However, presently available radio images of the field of NGC 1313 X-2 (Sydney University Molonglo Sky Survey at 843 MHz and Australia Telescope Array at ~ 5 GHz; Stocke et al. 1995) are not sufficiently deep to allow detection.

Optical spectroscopy of object C, narrow band imaging of the nebula, deep radio observations and an analysis of the short timescale X-ray variability are essential to better assess the physical properties of NGC 1313 X-2 and its environment. In particular, even a moderate resolution spectrum of object C will make it possible to detect any characteristic absorption and/or emission line, and then determine its properties and redshift. These observations will allow us to strengthen the identification of NGC 1313 X-2 with an intermediate mass BH and foster our under-

standing of ULXs.

We would like to thank Valentina Braito for her valuable help with some technical aspects involved in the analysis of *XMM* and *ASCA* data and the Padova-Asiago Supernova Group (in particular Andrea Pastorello) for providing us the ESO image of SN 1978K. We are also grateful to Steve Murray for allowing the *Chandra* observation of NGC 1313 X-2 to be taken as part of his GTO program, and to Albert Kong for carefully reading the manuscript and pointing out the possibility to reduce the *XMM* EPIC-PN data with the latest release of XMM-SAS. PK acknowledges partial support from NASA grant NAG5-7405 and Chandra grant GO2-3102X. This work has been partially supported also by the Italian Ministry for Education, University and Research (MIUR) under grants COFIN-2000-MM02C71842 and COFIN-2002-027145.

REFERENCES

Bohlin, R.C., Savage, B.D., & Drake, J.F. 1978, *ApJ*, 224, 132
 Bowers, R.L., & Deeming, T. 1984, *Astrophysics: Volume 1 – Stars* (Jones and Bartlett Publishers, Inc.)
 Brusa, M., Comastri, A., Daddi, E., Cimatti, A., Mignoli, M., & Pozzetti, L. 2002, *ApJ*, 581, L89
 Cagnoni, I., et al. 2002, *ApJ*, 579, 148
 Cagnoni, I., et al. 2003, *ApJ*, 582, 654
 Calzetti, D., et al. 2000, *ApJ*, 533, 682
 Chiang, E., & Rappaport, S. 1996, *ApJ*, 469, 255
 Colbert, E.J.M., Petre, R., Schlegel, E.M., & Ryder, S.D. 1995, *ApJ*, 446, 177
 Colbert, E.J.M. & Mushotzky, R.F. 1999, *ApJ*, 519, 89
 Colbert, E.J.M., & Ptak, A.F. 2002, *ApJS*, 143, 25
 de Jong, J.A., van Paradijs, J., & Augusteijn, T. 1996, *A&A*, 314, 484
 Di Stefano, R., Paerels, F., & Rappaport, S. 1995, *ApJ*, 450, 705
 Fabbiano, G., & Trinchieri, G. 1987, *ApJ*, 315, 46
 Fabbiano, G. 1989, *ARA&A*, 27, 87
 Fabbiano, G., et al. 2003, *ApJ*, 584, L5
 Fabbiano, G., & White, N.E. 2003, in *Compact Stellar X-ray Sources*, eds., W. Lewin & M. van der Klis, Cambridge University Press (astro-ph/0307077)
 Foschini, L., et al. 2002a, *A&A*, 392, 817
 Foschini, L., et al. 2002b, *A&A*, 396, 787
 Frank, J., King, A.R., & Raine, D.J. 2002, *Accretion Power in Astrophysics* (Cambridge University Press)
 Gioia, I.M., et al. 1990, *ApJS*, 72, 567
 Goad, M.R., Roberts, T.P., Knigge, C., & Lira, P. 2002, *MNRAS*, 335, L67
 Hambly, N.C., Irwin, M.J., & MacGillivray, H.T. 2001, *MNRAS*, 326, 1295
 Iwamoto, K. et al. 1998, *Nature*, 395, 672
 Kaaret, P. et al. 2001, *MNRAS*, 321, L29
 Kaaret, P., Corbel, S., Prestwich, A.H., & Zelas, A. 2003, *Science*, 299, 365
 Kaplan, D.L., Kulkarni, S.R., & van Kerkwijk, M.H. 2003, *ApJ*, 588, L33
 King, A.R., Davies, M.B., Ward, M.J., Fabbiano, G., & Elvis, M. 2001, *ApJ*, 552, L109
 Makishima, K., et al. 2000, *ApJ*, 535, 632
 Masetti, N. 1997, PhD Thesis, unpublished (<http://www.bo.iasf.cnr.it/~masetti/phdth.html>)
 Matonick, D.M., & Fesen, R.A. 1997, *ApJS*, 112, 49
 Miller, S., Schlegel, E.M., Petre, R., & Colbert, E. 1998, *AJ*, 116, 1657
 Miller, J.M., Fabbiano, G., Miller, M.C., & Fabian, A.C. 2003, *ApJ*, 585, L37
 Paczyński, B. 1971, *ARA&A*, 9, 183
 Pakull, M.W., & Mirioni, L. 2002, in *Proc. ESA Symp., New Visions of the X-ray Universe in the *XMM-Newton* and *Chandra* Era*, eds. F. Jansen et al. (ESA SP-488) (astro-ph/0202488)
 Petre, R., et al. 1994, *PASJ*, 46, L115
 Pickles, A.J. 1998, *PASP*, 110, 863
 Roberts, T.P., et al. 2001, *MNRAS*, 325, L7
 Ryder, S. et al. 1993, *ApJ*, 416, 167
 Schlegel, E.M., Petre, R., Colbert, E.J.M., & Miller, S. 2000, *AJ*, 120, 2373
 Shimura, T., & Takahara, F. 1995, *ApJ*, 445, 780
 Stocke, J.T., et al. 1995, *AJ*, 109, 1199
 Tully, R.B. 1988, *Nearby Galaxies Catalog* (Cambridge: Cambridge University Press)
 van der Marel, R.P. 2003, *Carnegie Observatories Astrophysics Series*, Vol. 1: *Coevolution of Black Holes and Galaxies*, ed. L. C. Ho (Cambridge: Cambridge Univ. Press), astro-ph/0302101
 Wu, H., Xue, S.J., Xia, X.Y., Deng, Z.G., & Mao, S. 2002, *ApJ*, 576, 738
 Zampieri, L., Turolla, R., & Szuszkiewicz, E. 2001, *MNRAS*, 325, 1266
 Zaritsky, D., Kennicutt, R.C., & Huchra, J.P. 1994, *ApJ*, 420, 87

TABLE 1
POSITIONS OF NGC 1313 X-2 AND POSITIONS AND OPTICAL MAGNITUDES OF FIELD OBJECTS

Observatory/Instr.	Object ^a	RA[J2000]	DEC[J2000]	R magnitude (Bessel-Cousins)	Ref.
<i>ROSAT</i> /HRI	NGC 1313 X-2	03 18 22.00 \pm 0.50	-66 36 02.3 \pm 3.0	—	Schlegel et al. (2000)
<i>XMM</i> /EPIC-MOS	NGC 1313 X-2	03 18 22.34 \pm 0.33	-66 36 03.7 \pm 2.0	—	Miller et al. (2003)
<i>Chandra</i> /ACIS-S	NGC 1313 X-2	03 18 22.18 \pm 0.12	-66 36 03.3 \pm 0.7	—	this work
ESO/3.6m	A	03 18 21.97 \pm 0.05	-66 36 06.5 \pm 0.3	19.8 \pm 0.2	this work
ESO/3.6m	B	03 18 21.56 \pm 0.05	-66 36 00.9 \pm 0.3	20.7 \pm 0.2	this work
ESO/3.6m	C	03 18 22.34 \pm 0.05	-66 36 03.7 \pm 0.3	21.6 \pm 0.2	this work
ESO/3.6m	D	03 18 20.96 \pm 0.05	-66 36 03.7 \pm 0.3	17.8 \pm 0.2	this work

^aSee Figure 3.

TABLE 2
PARAMETERS OF THE FIT OF *ROSAT*, *ASCA* AND *XMM* OBSERVATIONS

Observatory/Instr.	Obs. Id.	Model	N_H (10^{21} cm $^{-2}$)	Parameters	χ^2_{red} (dof)	F_X^a (10^{-12} erg cm $^{-2}$ s $^{-1}$)	$F_{0.2-10 \text{ keV}}^b$ (10^{-12} erg cm $^{-2}$ s $^{-1}$)
<i>ROSAT</i> /PSPC	rp600045n00	Power-law	1.06 $^{+2.14}_{-0.50}$	$\Gamma = 2.40^{+1.40}_{-0.60}$	0.83 (20)	1.4	2.6
		Blackbody	0.17 $^{+0.20}_{-0.15}$	$kT = 0.27^{+0.05}_{-0.03}$	1.01 (20)	0.34	0.38
<i>ROSAT</i> /PSPC	rp600504n00	Power-law	1.74 $^{+2.95}_{-1.31}$	$\Gamma = 2.20^{+1.50}_{-0.90}$	1.43 (22)	1.5	1.8
		Blackbody	0.09 $^{+0.09}_{-0.08}$	$kT = 0.35^{+0.05}_{-0.07}$	1.32 (22)	0.37	0.44
<i>ASCA</i> /GIS+SIS	60028000	Power-law	4.24 $^{+0.41}_{-0.41}$	$\Gamma = 1.99^{+0.03}_{-0.09}$	0.99 (171)	1.3	3.2
		MCD	1.15 $^{+0.35}_{-0.34}$	$kT = 1.38^{+0.07}_{-0.07}$	0.89 (171)	2.1	2.6
<i>ASCA</i> /GIS+SIS	93010000	Power-law	4.74 $^{+0.50}_{-0.50}$	$\Gamma = 2.43^{+0.09}_{-0.07}$	1.28 (139)	0.50	2.2
		MCD	1.06 $^{+0.31}_{-0.31}$	$kT = 1.08^{+0.04}_{-0.04}$	1.31 (139)	0.86	1.0
<i>XMM</i> /EPIC-MOS+PN	0106860101	Power-law	2.69 $^{+0.18}_{-0.16}$	$\Gamma = 2.42^{+0.07}_{-0.07}$	1.20 (249)	2.1	
		MCD	0.70 $^{+0.06}_{-0.06}$	$kT = 0.90^{+0.02}_{-0.02}$	2.29 (249)	0.86	
		CompTT ^c	1.67 $^{+0.43}_{-0.45}$	$kT = 3.00^{+0.11}_{-0.09}$ $T_0 = 0.15^{+0.03}_{-0.03}$ $\tau = 4.69^{+0.10}_{-0.10}$	1.11 (248)	1.2	
		MCD+Power-law	3.13 $^{+0.92}_{-0.37}$	$kT = 0.20^{+0.04}_{-0.05}$ $\Gamma = 2.23^{+0.15}_{-0.09}$	1.09 (247)	2.4	
		MCD+Power-law ^d	3.67 $^{+0.94}_{-0.52}$	$kT = 0.20^{+0.10}_{-0.07}$ $\Gamma = 2.23^{+0.12}_{-0.08}$	1.07 (247)	2.0	

^aUnabsorbed flux in the 0.1–2.0 keV (*ROSAT*), 2.0–10.0 keV (*ASCA*) and 0.2–10.0 keV (*XMM*) energy bands

^bUnabsorbed flux extrapolated in the 0.2–10.0 keV band using the web interface to PIMMS (v 3.3)

^cThermal comptonization model with Wien soft photon input

^dAbundance 0.5 solar

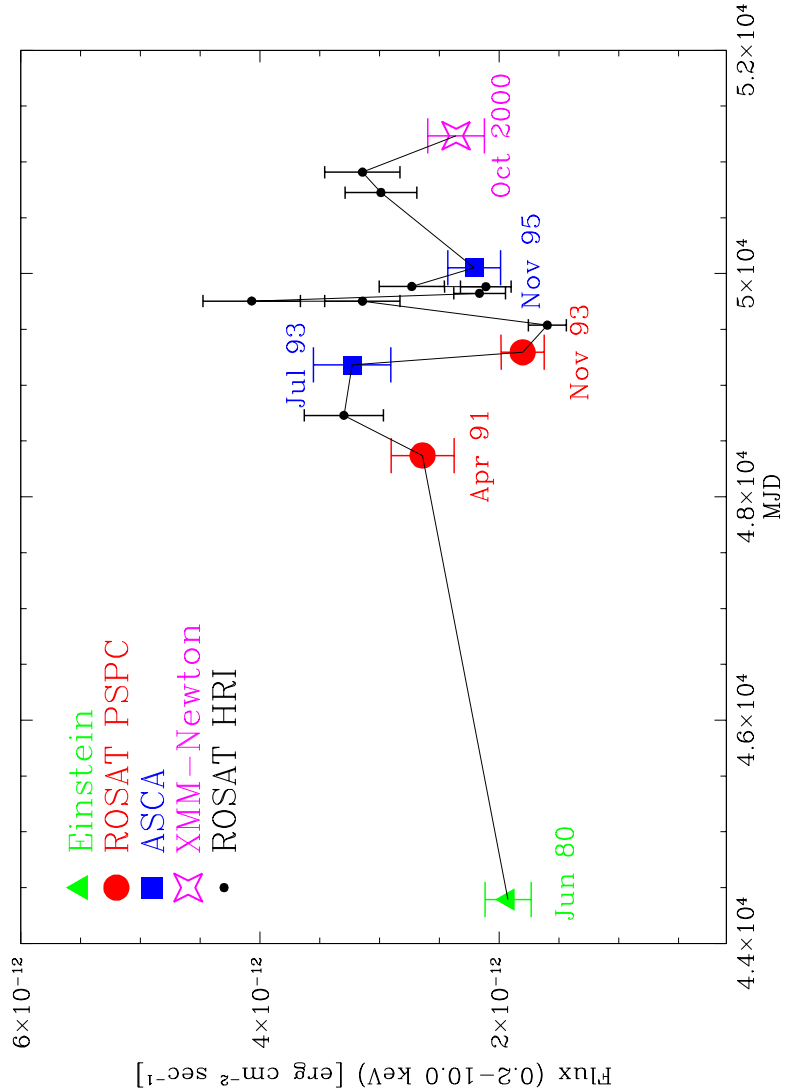


FIG. 1.— The 0.2-10 keV light curve of NGC 1313 X-2 from all presently available data. Fluxes were de-absorbed and, when necessary, extrapolated in the 0.2-10 keV interval using the web interface to PIMMS (see Table 2). For the *Einstein* IPC observation, we adopt the value reported by Gioia et al. (1990). For the *ROSAT* PSPC and *ASCA* GIS+SIS observations, the fluxes were derived from the best fit parameters of the power-law model reported in Table 2. For the *ROSAT* HRI data (Schlegel et al. 2000) a power-law spectrum with $\Gamma = 2$ and $N_H = 3 \times 10^{21} \text{ cm}^{-2}$ was assumed (in agreement with the best fit parameters derived from the spectral analysis). For the *XMM* EPIC data, the flux is calculated from the best fit MCD+power-law model reported in Table 2.

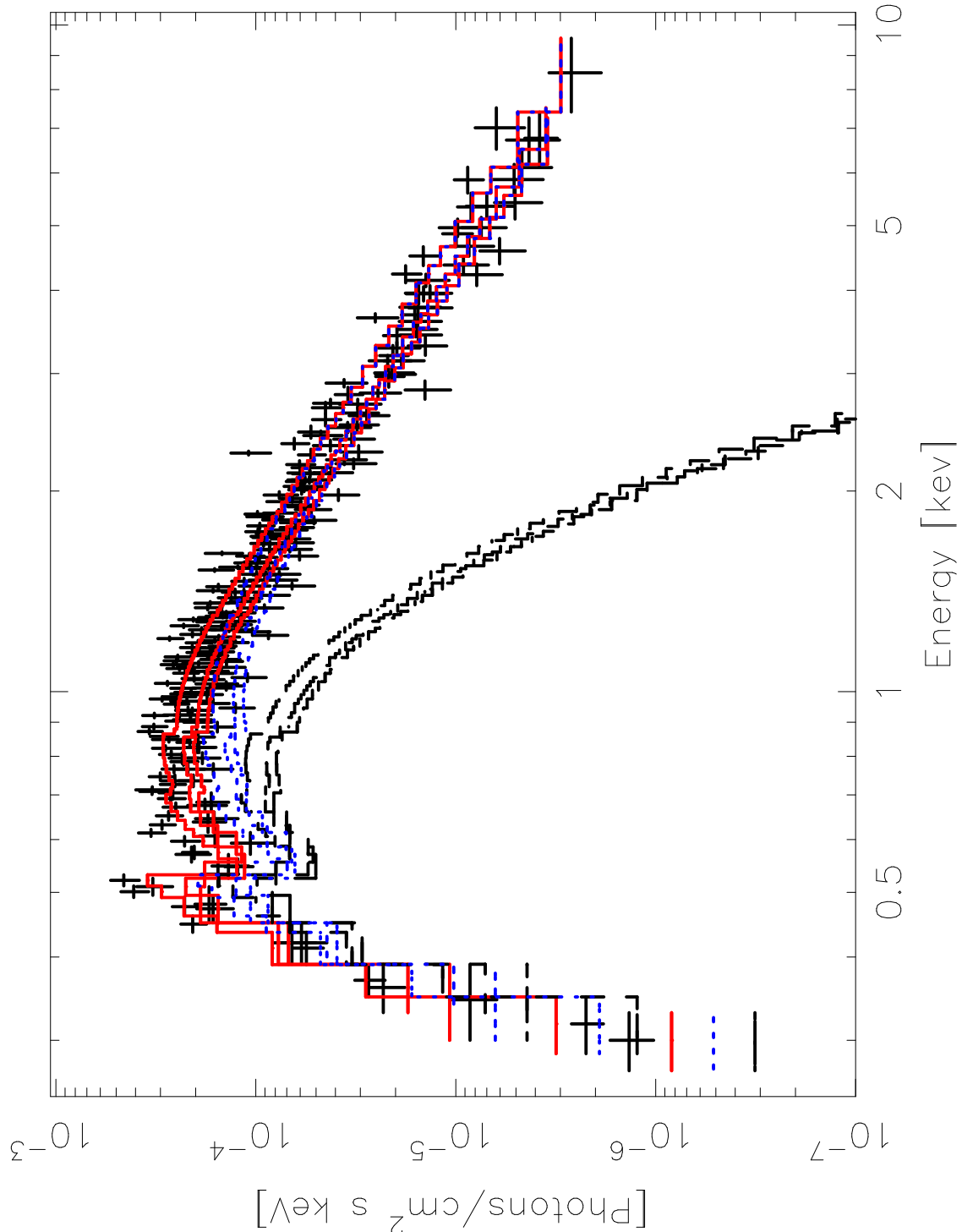


FIG. 2.— X-ray spectrum of NGC 1313 X-2 from the *XMM* EPIC-MOS and PN cameras. The solid line represents the combined best fitting model spectrum, while the dashed and dotted lines are the MCD and power-law components respectively.

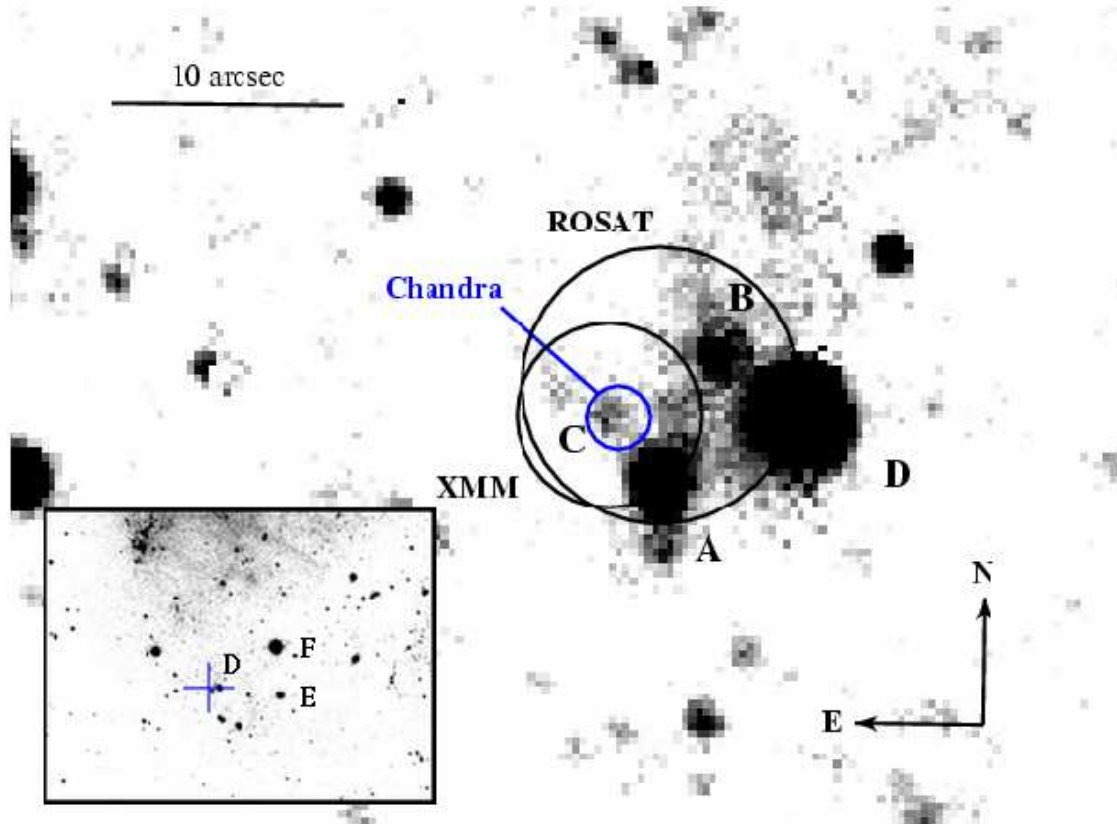


FIG. 3.— ESO 3.6m *R*-band (Bessel filter) image of the field of NGC 1313 X-2. The circles show the *ROSAT* HRI, *XMM* EPIC-MOS and *Chandra* ACIS-S positions. The estimated 90% confidence radii are 6'' for HRI, 4'' for EPIC-MOS and 1.4'' for ACIS-S. Labels A, B, C and D mark the four field objects inside or close to the X-ray error boxes. The insert at the bottom-left shows a larger portion of the image with the position of the X-ray source (cross).

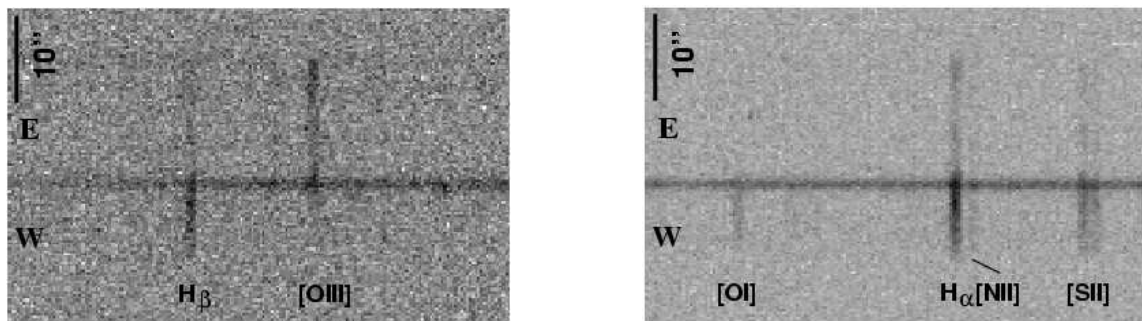


FIG. 4.— Two-dimensional spectrum (ESO 3.6m+EFOSC2+grism#4) of the field around object A. The slit (1.2'') is oriented in the east-west direction. The wavelength intervals are 4500–5300 Å (left panel) and 6150–6900 Å (right panel).

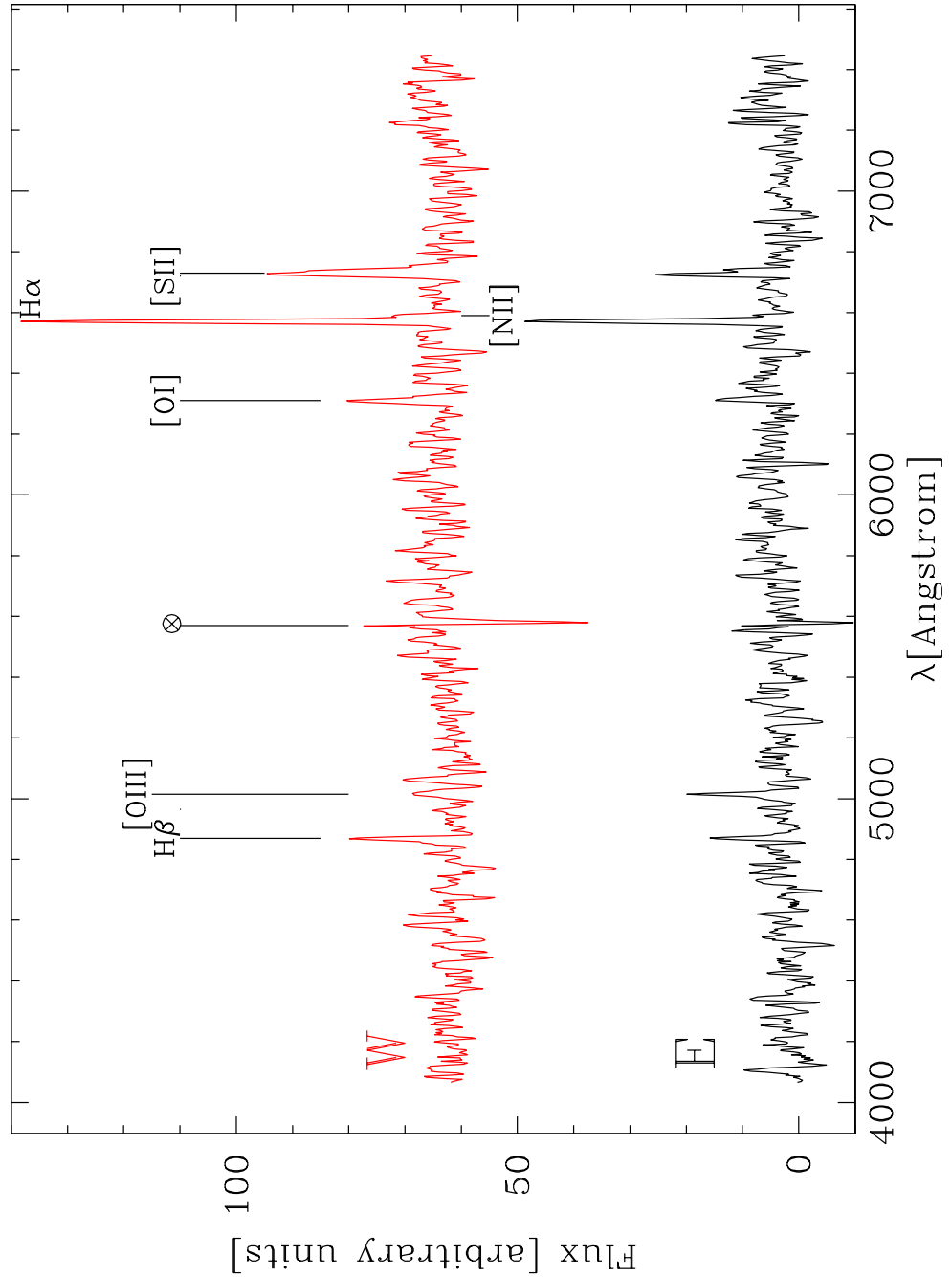


FIG. 5.— One-dimensional spectrum (F_λ) of the nebula around NGC 1313 X-2. The lower (upper) spectrum is extracted in a region east-ward (west-ward) of the position of object A (see text for details). The symbol \otimes marks a residual contamination from an emission line of the sky.

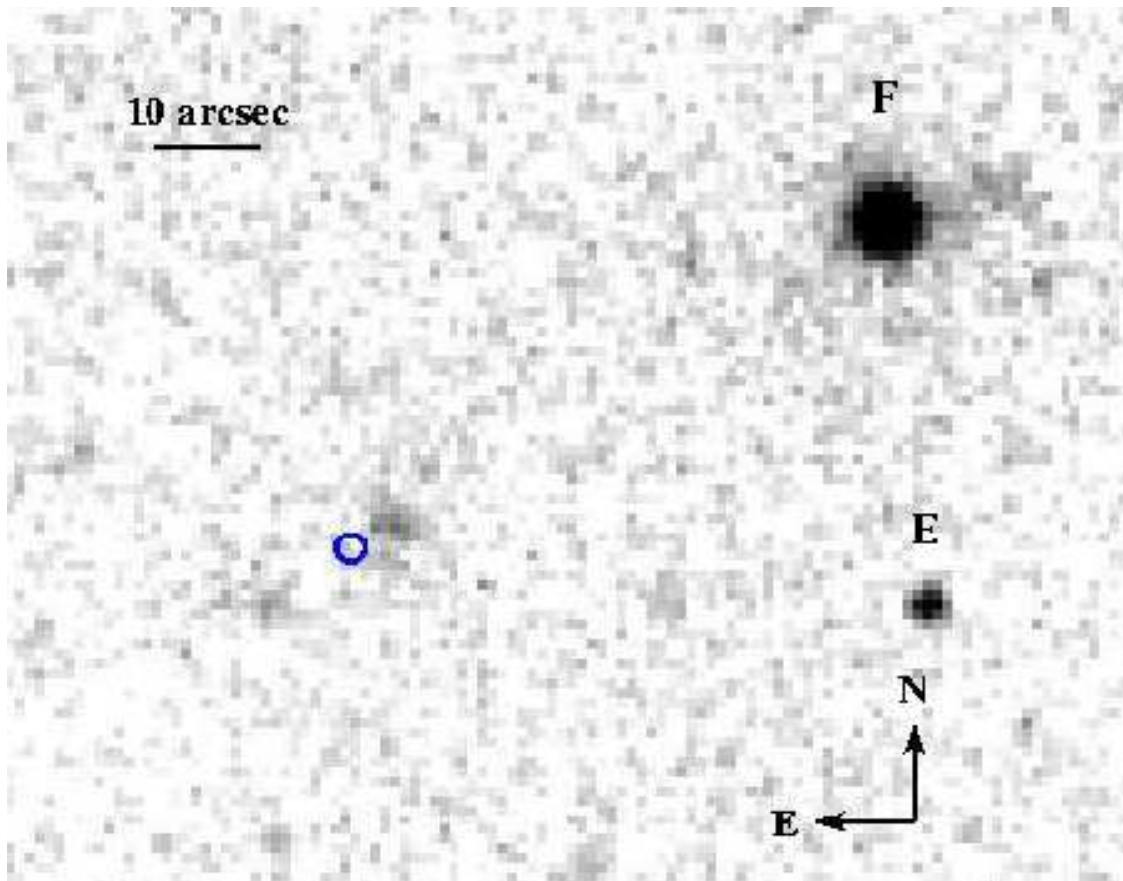


FIG. 6.—UV-band (UVW1 filter, 1800–3200 Å) exposure of the field of NGC 1313 X-2, obtained with the *XMM* Optical Monitor. The circle shows the *Chandra* position (90% confidence level). A region of possible diffuse emission is visible NW of the *Chandra* error box.